Rheology and scaling behavior of polyhedral particle flows in rotating drums

Duc Chung VU, Lhassan Amarsid, Jean-Yves Delenne, Vincent Richefeu, Farhang Radjai

Rheology and scaling behavior of polyhedral particle flows in rotating drums

Duc Chung Vu[a,b], Lhassan Amarsid[a], Jean-Yves Delenne[c], Vincent Richefeu[d], Farhang Radjai[b,*]

[a] *CEA, DES, IRESNE, DEC, SESC, LDOP, Saint Paul les Durance, 13108, France*
[b] *LMGC, CNRS, University of Montpellier, Montpellier, 34090, France*
[c] *IATE, INRAE, Institut Agro, University of Montpellier, Montpellier, 34000, France*
[d] *3SR, CNRS, University of Grenoble Alpes, Grenoble, 38400, France*

Abstract

We use particle dynamics simulations to investigate the rheology of granular flows composed of regular octahedral particles in a rotating drum. We focus on the cascading regime and perform an extensive parametric study by varying drum size, particle size, rotation speed, and filling degree. Our simulations indicate that the passive layer undergoes quasistatic shearing and, in contrast to spherical particle flows, no sliding occurs at the drum wall due to the angular particle shape. A scaling parameter combining the Froude number, the ratio of drum to particle size, and the filling degree captures the kinematic and dynamic characteristics of the granular flow such as free surface shape, shear velocity, flow thickness, and inertial number. This scaling suggests simple linear correlations between free surface curvature, flow thickness, and inertial number. We also show that this scaling is fully consistent with the expected effects of increasing particle size.

Keywords: Rotating drum, granular flow, cascading regime, polyhedral particle, scaling law, particle coarsening.

1. Introduction

The flow of granular materials inside a rotating drum is extensively applied in industrial processes such as mixing, grinding, granulation of granular materials. Although it has been studied by means of numerical models and experiments in recent years, there still remain open issues due to the complex and heterogeneous flow combining the upward rigid-body motion of the particles at the drum wall, downward bulk flow, and free surface dynamics [1, 2]. Drum flows are commonly classified into six different regimes: slipping, slumping, rolling, cascading, cataracting, and centrifuging [3, 4, 5]. These regimes are obtained by increasing the *Froude number*, $\mathrm{Fr} = \omega^2 R/g$, where ω is rotation speed, R is drum radius and g is gravity acceleration. The cascading regime provides a suitable particle flow configuration for industrial applications involving convection, mixing, segregation, and milling of particles [4, 6, 1, 7]. This is mainly due to the fact that this regime involves a continuous inertial flow of particles cascading downward due to gravity along a curved free surface and within a thick flowing layer [8, 1].

A major issue regarding drum flows is that they depend not only on the Froude number but also on other system parameters such as particle size and filling degree whose effect on the flow has not been fully understood [3, 9, 8]. Several scaling laws that include the system parameters have been proposed. For instance, Félix *et al.* [10] introduced a scaling law linking mean velocity $\langle v \rangle$ and thickness h_a of the active (flowing) layer through a power law $\langle v \rangle \sim h_a^m$, where the exponent m decreases with increasing size ratio D/d, with D and d being the drum and particle diameters, respectively. Pignatel *et al.* [11] found a constant value $m \simeq 1.27$ whereas Govender *et al.* [12] found $m \simeq 0.997$ in their work. By using theoretical and numerical models, Taberlet *et al.* [13] showed that the end walls are responsible for the curvature of the free surface, which is controlled by a dimensionless number including drum width, drum diameter, and rotation speed. In the case of wet granular flows of glass beads in rolling regime, Jarray *et al.* [14] found experimentally that dynamic angle of repose can be scaled by a parameter combining the Froude number and Weber number (ratio of inertial forces to capillary forces). The flow variables in the cascading regime were studied by Orozco *et al.* [1] who proposed a scaling by a single parameter that combines the Froude number, drum size D, particle size d, and filling degree J.

The above examples show that, although most previous studies have focused on the rolling regime and the flow of spherical particles, there are significant differences between the proposed scaling laws. Furthermore, the cascading regime has received much less attention and has been only recently studied on a systematic basis [1, 2]. Another important issue concerns the influence of particle shape on the flow regimes and more specifically on the behavior of the cascading regime [15, 16, 17, 18, 19]. With increasing computational power and optimization of contact detection algorithms, aspherical shapes are becoming accessible to large-scale particle dynamics simulations based on the Discrete Element Method (DEM). Examples of particles shapes that have been used in rotating drums for different applications are ellipsoids [20, 21, 22, 23], superquadrics [24, 25, 26], arbitrary-shaped clumps of spheres [27, 28, 29], and polyhedra [30, 31, 32, 33].

*Corresponding author:
Email address: franck.radjai@umontpellier.fr (Farhang Radjai)

Among these shapes, polyhedral particles are of primary importance since they are common in many applications and in nature, and also because arbitrary particles shapes can in principle be represented as polyhedra by meshing their surface into polygons. A key aspect of polyhedral particles is that they can interact through face-face, face-edge, vertex-face, and edge-edge contacts, which must be taken into account both in the contact detection procedure and for the calculation of forces. The distinction of contact types in drum flows has been addressed by a few recent DEM developments [24, 34, 7, 33].

In this paper, we use DEM simulations to analyze granular flows of octahedral particles in rotating drums in the cascading regime. The simulations are based on an original approach dealing properly with different contact types. We perform extensive simulations for a wide range of values of rotation speed, drum diameter, particle diameter, and filling degree. By a detailed analysis of flow variables such as the average and maximum slopes of free surface, flow thickness, shear rate, and inertia number in the flowing layer we find a dimensionless scaling parameter that accounts for the effect of all system parameters. In particular, we focus on the effect of particle-coarsening and we show that it is consistent with our scaling of flow variables. As we shall see, our scaling works also for spherical particles allowing thereby to highlight the effect of polyhedral particle shape through differences between model parameters.

In the following, we first introduce in Section 2 the numerical model and the procedures used to simulate drum flows. In Section 3, we describe the particle velocity fields and free surface profiles of drum flows. The scaling law of cascading flows will be proposed in Section 4. We also introduce a particle coarsening model in Section 5. Finally, we discuss the most salient results of this work in Section 6.

2. Numerical model and procedures

2.1. Simulation of polyhedral particles

The simulations were carried out by means of DEM in which polyhedral particles are treated as rigid bodies while the contacts between them are assumed to be compliant and obeying a viscoelastic behavior [35, 36, 37]. Polyhedral particles are transformed by means of Minkowski sum with a sphere of a small radius R_m [38]. This operation smoothens the polyhedra by replacing all edges by thin cylinders and all vertices by spheres. As a consequence, each polyhedron consists of three sub-elements, namely vertices which are small spheres of radius R_m, edges which are cylinders of radius R_m connecting two vertices, and faces which are planes of thickness $2R_m$ connecting at least three vertices.

The contacts between two polyhedra are represented by the contacts of its sub-elements, leading to six contact types: vertex-face, edge-edge, vertex-edge, vertex-vertex, edge-face, face-face. The unilateral constraint associated with these contact types do not have the same nature. The vertex-face, vertex-edge, vertex-vertex, and edge-edge interactions involve a single contact point, which can be treated in the same way as the contacts between spherical particles. Such simple contacts represent a single unilateral constraint as shown in Figs 1a and 1b. In contrast, a face-face contact is a plane that needs at least three points for its definition. Therefore, a face-face contact is equivalent to three simple contacts or unilateral constraints [37, 39]. This means that at least three contact points are necessary to represent the contact. Note that, the number of contact points can be larger depending on the number of edges as illustrated in Fig. 1d, but the number of independent constraints is always 3 since the particles are rigid. In a similar vein, edge-face interactions need two contact points as shown in Fig 1c. For this reason, edge-face and face-face contacts can be described as 'double' and 'triple' contacts, respectively.

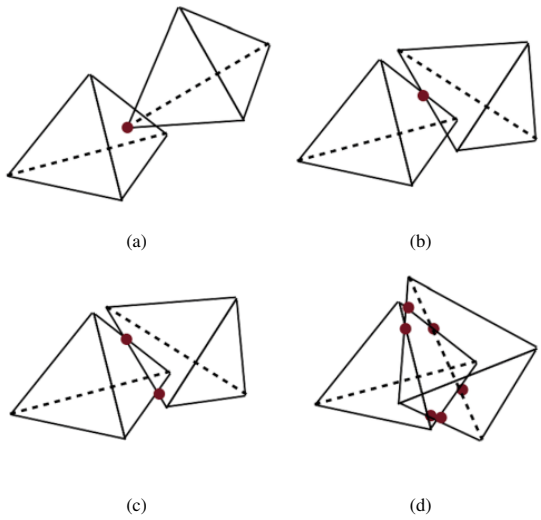

Figure 1: Different types of contacts between two polyhedra: (a),(b) simple contact, (c) double contact, and (d) triple contact.

At each contact point, either a linear or a nonlinear force law is implemented. For smooth particle surfaces with well-defined curvatures at the contact point, the Hertz law can be used. However, in this paper due to the faceted shape of particles, we used linear elastic law which is equivalent to a linear unilateral spring acting the the contact point. To account for contact inelasticity, a viscous damping term is added to the normal elastic repulsion force. Let $\vec{n}$ and $\vec{t}$ be the normal and tangential unit vectors at a contact point c between particles i and j. The force $\vec{f} = f_n\vec{n} + f_t\vec{t}$ acting by particle j on particle i is expressed as a function of the normal overlap δ_n and cumulative tangential displacement $\vec{\delta}_t$. The normal force law is defined as follows [35, 40]:

$$f_n = \begin{cases} 0, & \tilde{f}_n \leq 0, \\ \tilde{f}_n, & \tilde{f}_n > 0, \end{cases} \tag{1}$$

where $\tilde{f}_n = k_n\delta_n - 2a\sqrt{k_n m}\dot{\delta}_n$, k_n is normal stiffness, δ_n is overlap (with sign convention that $\delta_n > 0$ when two particle overlap), $\dot{\delta}_n$ is the relative normal velocity, m is reduced mass of two touching particles, and a is the dimensionless damping parameter which can take a value between 0 and 1. For $a = 0$, the contact is fully elastic whereas for $a = 1$ the contact is fully inelastic. In binary collisions, the normal restitution coefficient is a decreasing function of a [41, 42]. It is noteworthy that energy dissipation in dense granular flows is a collective multicontact process that involves elastic wave propagation across the

system. Typically low-frequency vibration modes are damped slowly in DEM calculations. For this reason, in DEM simulations of dense granular flows it is convenient to enhance contact dissipation by setting the restitution coefficient to a value close to zero (i.e. a close to 1). In our simulations, we set the coefficient of restitution to 0.001.

The tangential force f_t is governed by the Coulomb friction law:

$$f_t = min\{|k_t\vec{\delta}_t|,\ \mu_s f_n\}, \tag{2}$$

where k_t is tangential stiffness, δ_t is cumulative tangential displacement, and μ_s is the interparticle friction coefficient. The orientation of the tangential force $\vec{t}$ is opposite to either the relative elastic displacement $\vec{\delta}_t$ below the Coulomb threshold or the relative velocity $\vec{v}_t$ at the contact point when the Coulomb threshold is reached.

2.2. Sample setup and boundary conditions

We consider horizontal drums of diameter $D = 2R$ and width W filled with monodisperse octahedral particles of diameter d, and subjected to rotation speed ω as illustrated in Fig. 2a. We used a monodisperse system to avoid introducing unnecessary parameters. Note also that long-range ordering in monodisperse systems is a pathology of 2D systems. A packing of monodisperse particles in 3D does not develop long-range ordering. Octahedral particle shape was chosen due to its high angularity, distinguishing it from spherical shape [37]. Periodic boundary conditions are imposed along the drum axis y to reduce wall effects. This makes the flow invariant along the y axis. The filling degree is defined by the ratio $J = h_0/D$, where h_0 is the thickness of granular material at the midpoint of the free surface at rest. The friction coefficients between particles and with drum wall are set to $\mu = 0.4$, which is a common value used for smooth drum wall [1, 43].

The simulations were carried out for a broad range of values of ω, D, d, and J as shown in Table 1. As we shall see, the selected ranges of these parameters the flow is in the cascading regime. In order to isolate the effect of drum size, particle size and filling degree, we performed four sets of simulations. In the first set (set A), drum diameter D was changed for $d = 0.682$ mm and $J = 0.40$. In the second set (set B), d was varied for $D = 40$ mm and $J = 0.40$. In the third set (set C), J was changed for $D = 40$ mm and $d = 0.682$ mm. Furthermore, to verify the accuracy of the scaling law that will be discussed in this paper, we performed more simulations by changing all parameters simultaneously (set D).

The simulations were run for at least 10 drum rotations to allow the system to reach a steady flow state. The data analyzed in this paper, such as the free surface profile, flow thickness, relative particle velocities, flow rate, and inertia number are averaged over time in the steady state.

3. Particle velocity fields and free surface profiles

A snapshot of particle velocity vectors in a rotating drum of size ratio $D/d = 81$, and the free surface for different size ratios, but with the same filling degree J and rotation speed ω, are displayed in Fig. 3. The largest velocities are located at the center of free surface where particles are cascading down, and they increase in magnitude with drum size despite the constant value of rotation speed ω. We see that for all values of size ratio the flow is in the cascading regime with a free surface curvature that increases with size ratio.

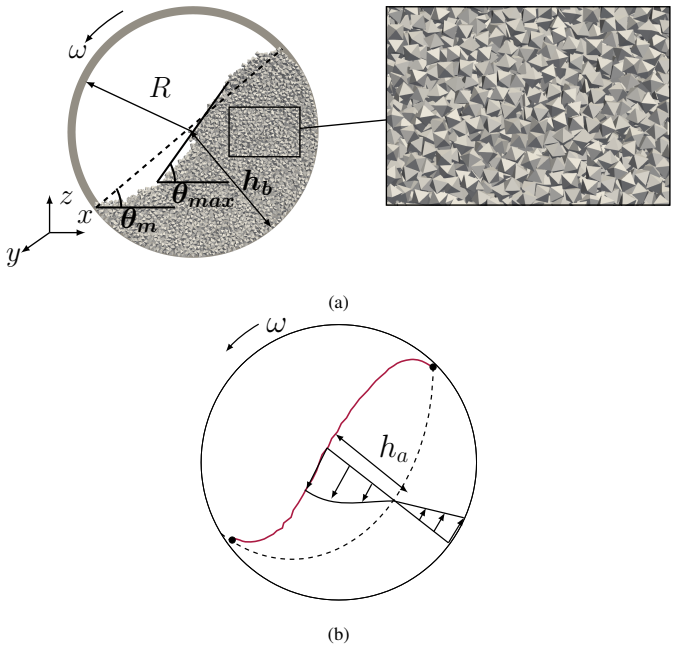

Figure 2: Geometrical parameters of granular flow in rotating drum in the steady state (a), and particle velocity profile along the bed depth direction in the center of the cylinder (b).

Two examples of averaged particle velocity fields in drums of different size ratios are displayed in Fig. 4. The velocity vectors are projected on the secant slope. Positive values correspond to particles flowing downward under the effect of gravity whereas negative values correspond to upward motion of the particles. From the velocity field, we clearly distinguish the active layer (upper) from the passive layer (lower). The passive layer behaves as a solid body undergoing slow deformation against the

Parameter	Symbol	Value	Unit
Number of particles	N_p	[2522; 18392]	-
Particle density	ρ_s	1.2×10^4	kg/m^3
Normal stiffness	k_n	10^8	N/m
Tangential stiffness	k_t	8×10^7	N/m
Restitution coefficient	e_n^2	0.001	-
Friction coefficient	μ	0.4	-
Gravity acceleration	g	9.81	m/s^2
Mean particle diameter	d	[0.682; 1.092]	mm
Rotation speed	ω	[10; 20]	rad/s
Drum diameter	D	[30; 55]	mm
Drum width	W	6	mm
Froude number	Fr	[0.12; 0.70]	-
Filling degree	J	[0.29; 0.40]	-

Table 1: Simulation parameters.

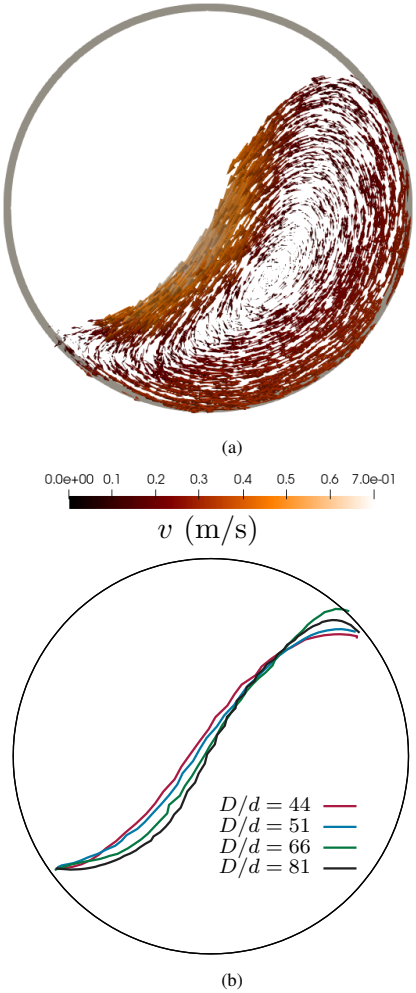

Figure 3: Velocity vector fields in drum of the size ratios $D/d = 81$ (a), the free surface in drums of different size ratios (b). The filling degree ($J = 0.4$), mean particle diameter ($d = 0.682$ mm), and rotation speed ($\omega = 12$ rad/s) are the same in all cases. The arrow length and color are proportional to particle velocity magnitude.

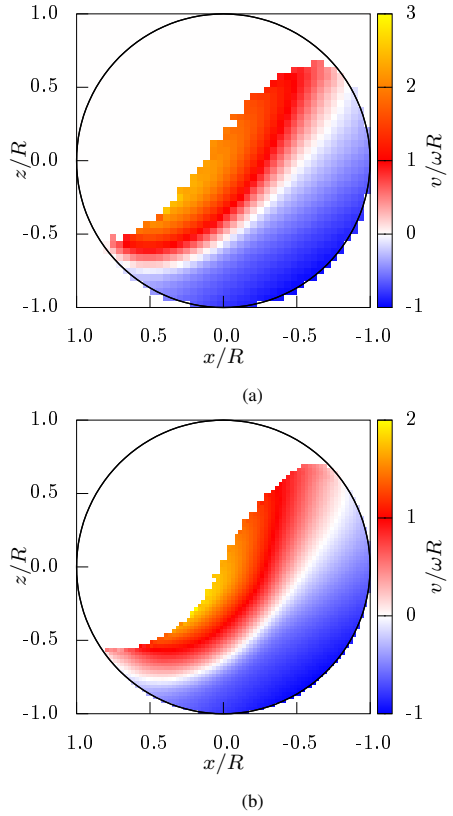

Figure 4: Time-averaged particle velocity field in drums of two different size ratios D/d of 44 (a) and 81 (b) for filling degree $J = 0.4$, mean particle diameter $d = 0.682$ mm, and rotation speed $\omega = 12$ rad/s in all cases. The particle velocity is projected on the secant slope defined by its angle θ_m.

drum wall. When the particles reach the free surface, they join the active layer at different positions above the borderline between the two layers, flow downward, and eventually rejoin the passive layer. We also see the boundary at the interface between the active and passive layers. The flow thickness h_b is evaluated from the free surface along the line passing by the midpoint of the secant slope and perpendicular to it (see Fig. 2a). The secant line is defined by joining the uppermost point of the free surface to its lowermost point. The active layer thickness h_a is part of h_b, and is defined as the distance from the free surface to the interface between the active and passive layers (see Fig. 2b). The active layer thickness h_a is an important parameter for phenomena such as mixing, segregation, and heat transfer in rotating drums [3, 4] and it varies with system parameters in the cascading regime.

Figure 5 displays the velocity profile along the bed depth direction (with depth h measured from the free surface) for our three data sets (set A, set B, and set C). The particle velocity is projected on the secant slope defined by the angle θ_m. The profile in the passive layer is almost linear. From $v \simeq -0.5\omega R$ to $v \simeq 0$, we observe an intermediate region over which the transition to the active layer occurs. For $v > 0$, the particles are in the active layer and the velocity profile is again nearly linear [6, 24, 44]. The transition zone is the locus of convective rolls that accommodate strain fields between the passive and active layers as suggested by the particle velocity vectors shown in Fig 3. The thickness of this zone is nearly 5 particle diameters in the center of the drum. In Fig. 5(a) we observe that for $D/d = 74$ and $D/d = 81$ the velocity profile tends to turn upward near the free surface, deviating from the linear profile. This is due to the high value of Froude number and small size of the particles, which, as we shall see, lead to larger curvature of the free surface and increasing fluidization in the center of the flow. This deviation is a signature of transition to the cataracting regime in which the particles in the center of flow follow a ballistic motion.

It is noteworthy that the particle velocity of the layer in contact with the drum wall is close to ωR, implying that the particles do not slide along the drum wall. Slippage of particles against drum wall has been observed in the case of spherical particles. We also see that the ratio h_a/h_b, where h_b is the thickness of the flow in the center of the drum during flow, and the free surface curvature increase with increasing drum size [1]. On the other hand, the free surface velocity and the ratio h_a/h_b

decrease for larger particle sizes.

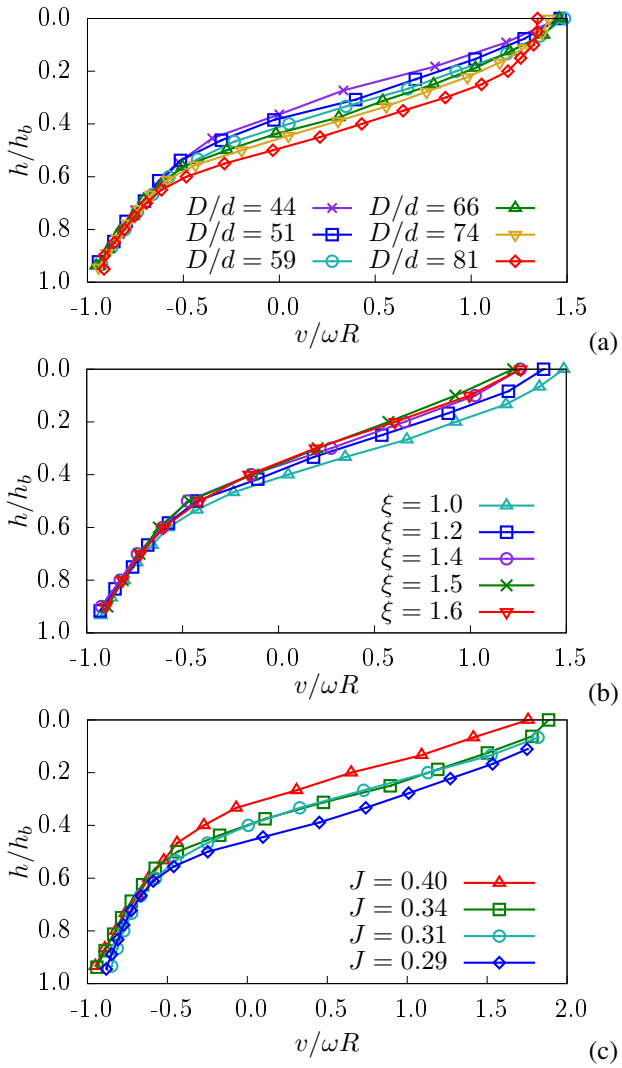

Figure 5: Time-averaged velocity profile in the center of the drum as a function of depth measured from the free surface and normalized by the total bed depth h_b for three data sets: (a) set A (D is varied) with ω = 15 rad/s, d = 0.682 mm, (b) set B (d is varied) with ω = 15 rad/s, $\xi = d/d_0$, where d_0 = 0.682 mm, and (c) set C (J is varied) with ω = 10 rad/s, d = 0.682 mm. The particle velocity is projected on secant slope and normalized by ωR.

To characterize the free surface shape, we define two slope angles: the secant slope θ_m and the tangent slope θ_{max} of the steepest descent along the free surface, as shown in Fig. 2a. The secant slope represents the average slope of the free surface. The angle θ_{max} reflects the kinematics of the free surface flow and the flow rate due to the amount of feeding particles. The rotation speed ω or Froude number Fr are insufficient to capture the evolution of θ_m and θ_{max} [9, 1]. The slope ratio θ_{max}/θ_m represents a measure of the curvature of the slope. Its significance appears through its scaling with system parameters, as we shall see below.

The evolutions of slope ratio θ_{max}/θ_m and thickness ratio h_a/h_b as a function of size ratio D/d are shown in Fig. 6 for data set A with four values of ω. We see that both ratios increase with drum size and with rotation speed in agreement with previous studies [1]. Note that all data points shown in Fig. 6 are in the cascading regime. The maximum values reached are θ_{max}/θ_m = 1.7 and h_a/h_b = 0.5. Beyond this limit, a crossover is observed from cascading flow to cataracting flow. By definition, in the rolling regime we have θ_{max}/θ_m = 1. Hence, it is expected that the lowest value of this ratio is 1 and occurs at crossover from rolling regime to cascading regime. However, in Fig. 6 we see that the lowest value is ~ 1.3. This point will be discussed in Sec. 4.

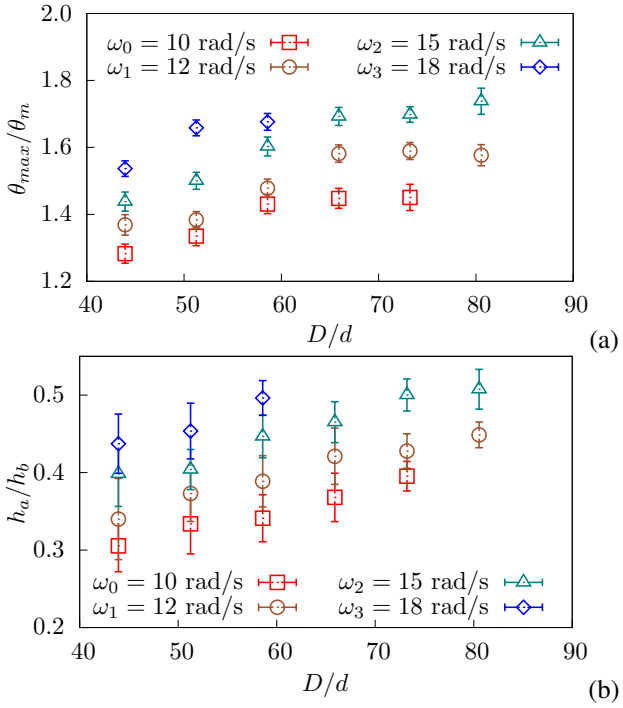

Figure 6: The ratios (a) θ_{max}/θ_m and (b) h_a/h_b as a function of size ratio D/d for different rotating speeds ω for d = 0.682 mm and variable drum diameter D. The error bars represent standard deviation in steady flow.

Let us define v_r as the relative velocity of particles in contact with drum wall:

$$v_r = \omega R - v_w, \tag{3}$$

where v_w is the time-averaged velocity of particles in contact with drum wall in the steady state. Figure 7 shows v_r as a function of the relative velocity $\dot{\gamma}_p d$, where $\dot{\gamma}_p$ is shear rate in the passive layer. We see that v_r increases with and is nearly equal to $\dot{\gamma}_p d$. This means that the value of v_w is mainly controlled by shearing in the passive layer rather than sliding against the drum wall. The absence of sliding at the drum wall can be attributed to the lower mobility of polyhedral particles as compared to spherical particles [1, 13]. In the rolling regime, where wall sliding is often observed, v_r is much higher than $\dot{\gamma}_p d$ [45].

Since there is almost no sliding at the wall, mass conservation implies that the upward flux of particles in the passive layer must be equal to the downward flux in the active layer. Let us consider the flow rate per unit of width $Q = \Phi v h$, where Φ, v, and h are solid fraction, average velocity and thickness of a layer, respectively. In the passive layer, the average flow rate is given by $Q_p \simeq \langle\Phi_p\rangle(h_b - h_a)\langle v_p\rangle$, where $\langle\Phi_p\rangle$ and $\langle v_p\rangle$ are the

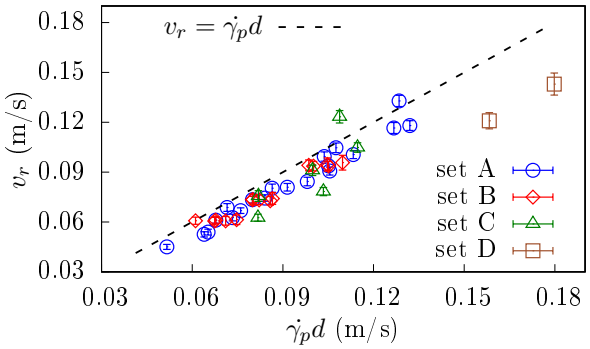

Figure 7: The relative velocity of particles in contact with drum wall as a function of the relative velocity $\dot{\gamma}_p d$ inside the passive layer for a range of different values of drum diameter D and particle diameter d.

average solid fraction and velocity, respectively, in the passive layer evaluated for the whole period of flow. In the same way, in the active layer, the average flow rate is $Q_a \simeq \langle \Phi_a \rangle h_a \langle v_a \rangle$, where $\langle \Phi_a \rangle$ and $\langle v_a \rangle$ are the average solid fraction and velocity, respectively, in the active layer. Figure 8 shows $Q_a/(d\sqrt{gd})$ as a function of $Q_p/(d\sqrt{gd})$ for all our datasets. We see that all data points collapse well on the $Q_a/(d\sqrt{gd}) = Q_p/(d\sqrt{gd})$ line. This confirms that sliding at the wall is negligible. Deviations are due to the fact that the flow profile is not symmetric around the secant line used to define the average direction of flow and the interface between the passive and active layers fluctuates in time.

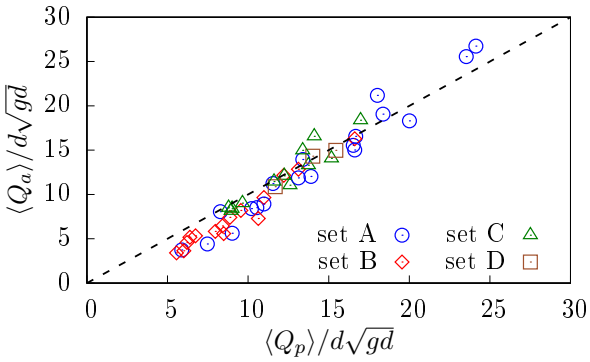

Figure 8: Dimensionless flow rate Q_a in the active layer as a function of dimensionless flow rate Q_p in the passive layer, both normalized by $d\sqrt{gd}$, where g is gravity acceleration. The dashed line represents the line $Q_a/(d\sqrt{gd}) = Q_p/(d\sqrt{gd})$.

4. Scaling behavior of cascading flows

Dimensional analysis suggests that the flow behavior depends on three dimensionless numbers: (1) Froude number, which accounts for the dynamics and inertial effects, (2) size ratio D/d accounting for finite-size effects, and (3) filling degree J characterizing the geometry of the flow. As suggested previously for spherical packings [1], we look for a general dimensionless scaling parameter based on a multiplicative combination of the above three parameters:

$$\Gamma = \mathrm{Fr}^{\alpha} \left(\frac{D}{d}\right)^{\beta} J^{\gamma}, \tag{4}$$

where the exponents α, β, and γ will be fixed from the simulation data. Since $J = h_0/D$ and $\mathrm{Fr} = \omega^2 R/g$, the scaling parameter Γ is proportional to $\omega^{2\alpha} D^{\alpha+\beta-\gamma} d^{-\beta}$.

To find the values of the three exponents, we can use any dynamical variable of the system as a function of Γ. The value of α can be calculated by plotting the relation between v_r and ω while keeping other system parameters constant. In Fig. 9, we plot the normalized velocity $v_r/\sqrt{gd}$ as a function of ω for different values of drum size D with the same values of d and J. We see that $v_r/\sqrt{gd}$ is proportional to ω so that $\alpha = 1/2$. The value of β can be extracted from the relation of v_r and d while keeping D, J, and ω at constant values. Figure 10 shows that v_r is independent of d, meaning that $v_r/\sqrt{gd} \sim d^{-1/2}$, and thus we have $\beta = 1/2$.

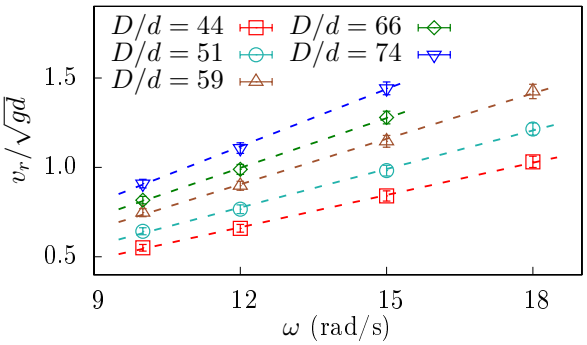

Figure 9: The normalized relative velocity of particles in contact with drum wall as a function of rotation speed ω for different values of drum diameter D and constant mean particle diameter $d = 0.682$ mm and filling rate $J = 0.40$.

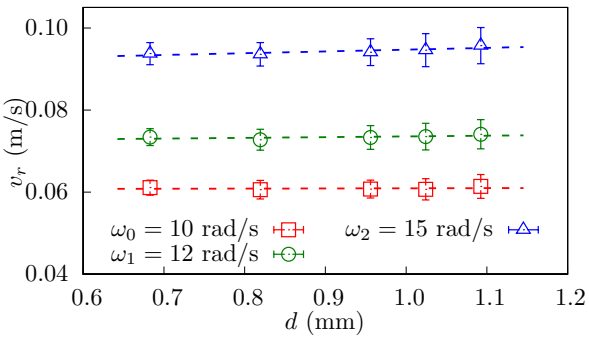

Figure 10: Relative velocity of particles at drum wall as a function of mean particle diameter d for different values of rotation speed ω and constant drum diameter $D = 40$ mm and filling rate $J = 0.40$.

With the values $\alpha = 1/2$ and $\beta = 1/2$, we plotted normalized relative velocity $v_r/\sqrt{gd}$ as a function of Γ for all our simulation data and we found that all the data collapse on a master curve for $\gamma = 1/4$, as shown in Fig. 11. Furthermore, this curve is a linear function:

$$\frac{v_r}{\sqrt{gd}} \simeq 0.29\Gamma - 0.05. \tag{5}$$

This simple relation suggests that $\Gamma = \mathrm{Fr}^{1/2}(D/d)^{1/2}J^{1/4}$ can be the scaling parameter not only for v_r but for all flow variables of the system. Indeed, as shown in Fig. 12, within statistical precision of the simulation data, both the thickness ratio h_a/h_b and slope ratio θ_{max}/θ_m are well fit to linear functions of Γ for all our simulation data:

$$\frac{h_a}{h_b} \simeq 0.07\Gamma + 0.16, \tag{6}$$

and

$$\frac{\theta_{max}}{\theta_m} \simeq 0.15\Gamma + 1.00. \tag{7}$$

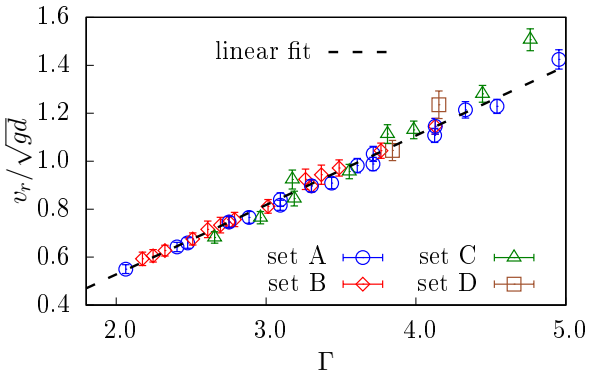

Figure 11: The normalized velocity of particle in contact with drum wall as a function of the scaling parameter Γ defined by Eq. (4) with $\alpha = 1/2, \beta = 1/2, \gamma = 1/4$ for all simulation data.

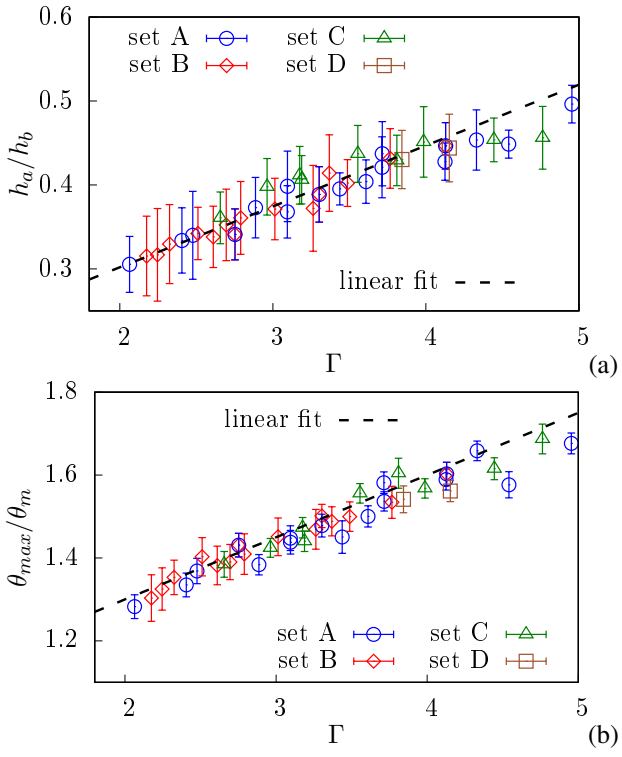

Figure 12: Thickness ratio h_a/h_b (a) and slope ratio θ_{max}/θ_m (b) as a function of the scaling parameter Γ defined by Eq. (4) with $\alpha = 1/2, \beta = 1/2, \gamma = 1/4$ for all simulation data. The dashed lines are fitted lines proposed.

We also note that in Fig. 12 the data points at higher values of Γ seem to deviate from the above general scaling. This observation suggests that these points are at the crossover from cascading regime to cataracting regime. These deviations occur when h_a/h_b approaches 0.5 and θ_{max}/θ_m reaches 1.7, corresponding therefore to the thickest flow layers and highest slopes. It is noteworthy that previous studies of the rolling regime have indicated that the transition from rolling to cascading regime occurs at $h_a/h_b \simeq 0.3$, which corresponds to $\Gamma \simeq 2$ as seen in Fig. 12 [4, 46]. Hence, according to our data for octahedral particles, the cascading regime is limited to the range of values of Γ from 2 to 5 independently of the specific values of ω, D, d, and h_0.

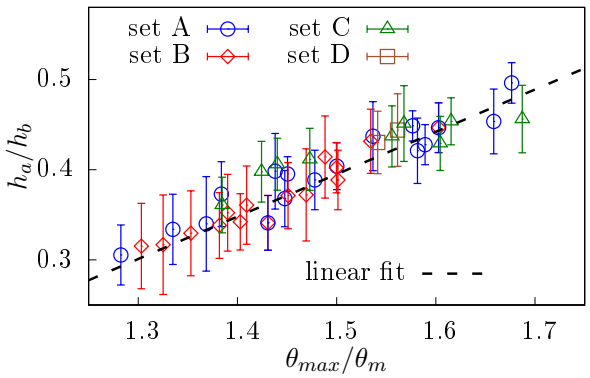

Figure 13: The ratio θ_{max}/θ_m versus the ratio of active layer thickness to total thickness h_a/h_b for all our data points. The dashed line shows the prediction of the scaling relation in Eq. (8).

The above scaling suggests that all flow variables are connected together through their dependence on Γ. For example, the ratio θ_{max}/θ_m as a kinematic property of drum flow is correlated with the active layer thickness ratio h_a/h_b, which is a dynamic property of the flow. Our scaling predicts the following relation:

$$\frac{h_a}{h_b} \simeq 0.47\frac{\theta_{max}}{\theta_m} - 0.31. \tag{8}$$

This relation is in excellent agreement with our data as shown in Fig. 13.

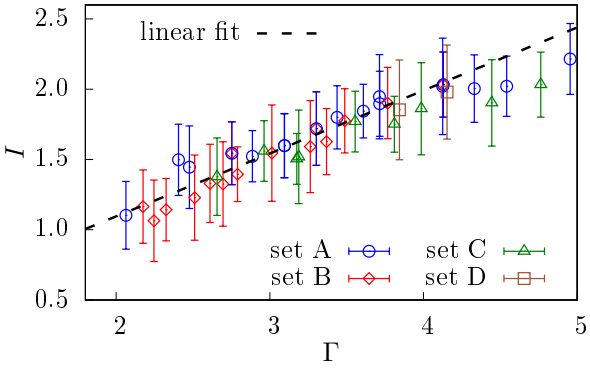

Figure 14: Average inertia number in the center of the active layer I as a function of scaling parameter Γ defined by Eq. (4) with $\alpha = 1/2, \beta = 1/2, \gamma = 1/4$ for all simulation data.

Another important flow variable is the average inertia number I in the active layer. It is defined as follows:

$$I = \langle \dot{\gamma}_a \rangle d(\rho_s/p)^{1/2}, \tag{9}$$

where $\langle \dot{\gamma}_a \rangle$ is average shear rate in the center of the active layer, ρ_s is particle density, and $p \simeq 0.5\langle \Phi_a \rangle \rho_s g h_a$ is the average pressure in the center of the active layer. Figure 14 shows that I is scaled quite well by Γ with the following linear relation:

$$I \simeq 0.45\Gamma + 0.2. \tag{10}$$

We see that I has generally high values and exceeds 2 at $\Gamma = 4$.

Similar scaling parameters have been proposed by other authors. In particular, Orozco *et al.* [1] found a different scaling parameter for their data obtained from simulations of rotating drums filled with spheres for periodic boundary conditions along drum axis to remove end wall effects. We consider here part of their data as a function of our scaling parameter Γ in order to compare the flows of polyhedra and spheres in the cascading regime. For comparison, we consider the data of Orozco et al. either at a constant value of the filling degree $J = 0.45$ or for changing values of J and ω. Figure 15 displays the evolution of slope ratio θ_{max}/θ_m for both octahedral and spherical drum flows versus the scaling parameter Γ in these two cases. We see that the data of spherical particles at $J = 0.45$ coincide well with those of octahedral particles. However, for variable J and ω and a constant size ratio D/d, the slope ratio for spheres increases with Γ but they do not fall on the scaling line of octahedral particles. We have no clear clue as to the origins of this discrepancy, but we believe that a full comparison is necessary to understand the differences for the two particles shapes with respect to all system parameters and the scaling behavior. In particular, the effect of the filling degree seems to be less well accounted for in the simulations of spheres. It is also important to remark that the ranges of values of Γ for which the flow is in the cascading regime is different for octahedral and spherical particle flows.

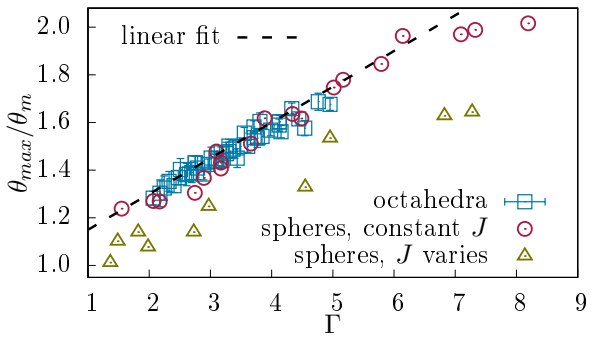

Figure 15: Slope ratio θ_{max}/θ_m as a function of scaling parameter Γ defined by Eq. (4) with $\alpha = 1/2$, $\beta = 1/2$, $\gamma = 1/4$ for simulation data of octahedral particles (this work) and spherical particles (data from Orozco *et al.* [1]) in which the filling degree J is kept constant or varies with other parameters kept constant.

5. Particle coarsening approach

The scaling parameter $\Gamma = \mathrm{Fr}^{1/2}(D/d)^{1/2}J^{1/4}$ extracted from our simulation data involves a dependence of cascading flow properties on particle size as $d^{-1/2}$. Here, we would like to show that this size dependence is consistent with the particle coarsening approach. In this approach, particle size is artificially scaled up by a factor ξ, i.e. $d \to d' = \xi d$, while keeping the size of the system, i.e. $D \to D' = \xi^0 D$, so that the total number of particles is reduced by a factor ξ^3 ($N_p \to N'_p = \xi^{-3}N_p$) [47, 48, 49]. The scaling of the dimensional quantities of the system depends on the variables that are assumed to be invariant functions of ξ. In general, we require that both macroscopic variables and system-scale quantities (boundary conditions and loading) are invariant by scale change. The physical rationale behind this assumption is that coarse-grained variables must be independent of particle size, which is a microscopic length of the system.

In application to rotating drum, we assume that drum size D, particle density ρ_s, and filling degree J are invariant. This implies that the total mass of the flowing particles is invariant. In the same way, the rotation speed ω, gravity g, and velocity field $\{\vec{v}\}$ are invariants of ξ. Consistently, it is easily seen that the total kinetic energy $E_{tot} = N_p(\langle mv^2/2 \rangle + \langle I_o \omega_o^2/2 \rangle)$, where I_o is the moment of inertia of the particle around its rotation axis and ω_o is angular speed around the axis, is also invariant since $N_p \to N'_p = \xi^{-3}N_p$, $m \to m' = \xi^3 m$, $v \to v' = \xi^0 v$, $I_o \to I'_o = \xi^5 I_o$, and $\omega_o \to \omega'_o = \xi^{-1}\omega_o$. In our simulations, we have 5 values of d which can be considered as upscaled diameters of the smallest particle size $d_0 = 0.682$ mm by coarsening factors $\xi = d/d_0$, which vary from 1 to 1.6. Figure 16 shows the total kinetic energy E_{tot} and relative velocity v_r for three different values of rotation speed as a function of ξ while all other parameters keep their values in set B. We see that both E_{tot} and v_r are invariant as a function of the coarsening factor ξ.

Regarding dynamic variables, since gravity g is invariant, momentum balance implies that particle weights and contact forces scale with ξ^3 while stresses vary as ξ. As a consequence, the inertial number in the active layer $I = \dot{\gamma}_a d\sqrt{\rho_s/p}$ varies as $I' = \xi^{-1/2}I$. This is fully consistent with the linear dependence of I on Γ in Eq. (10). Hence, the exponent $\beta \simeq 1/2$ in Eq. (4) is a natural consequence of coarse graining. Fig. 17 displays $\langle \dot{\gamma}_a \rangle d$ and $\xi^{1/2}(I - 0.2)$ as a function of ξ for the data set B for three different values of ω. We see that both variables are independent of ξ. The offset 0.2 in $I - 0.2$ has been added here to restrict the analysis to the cascading regime, in which the lowest value of I is 0.2. Note also that the invariance of $\langle \dot{\gamma}_a \rangle d$ simply reflects that of the velocity field. It implies that $\langle \dot{\gamma}_a \rangle$ varies as ξ^{-1} and thus also all times scale as ξ. This property of particle coarsening is well known in granular gases and leads to a decrease of collision rate and dissipation when particles are coarsened [50].

The dependence of inertial number on particle size leads to the variation of the free surface shape. Figure 18 shows snapshots of the particles in the drums at steady state with the same rotation speed ω, but different coarsening factors ξ. We see that the free surface becomes less curved as ξ increases. This is in

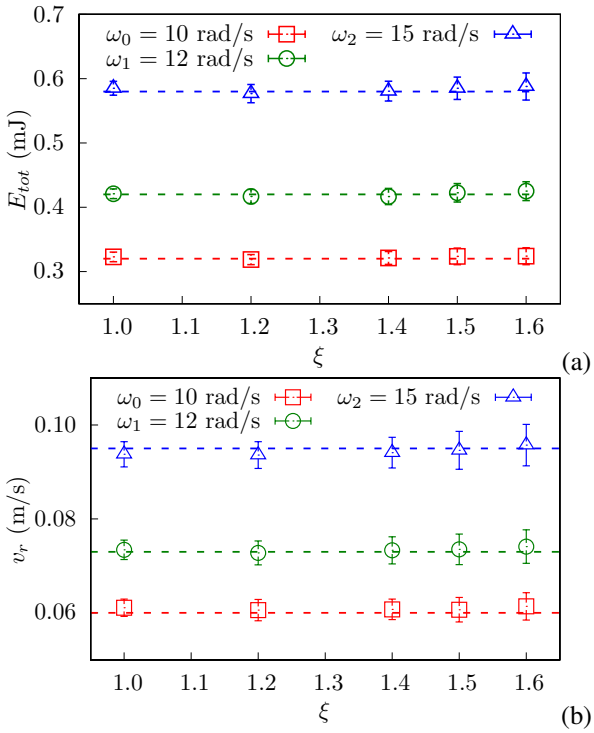

Figure 16: Total kinetic energy of particles E_{tot} and relative velocity of particles near drum wall v_r as a function of coarsening factor ξ. The error bars represent the standard deviation.

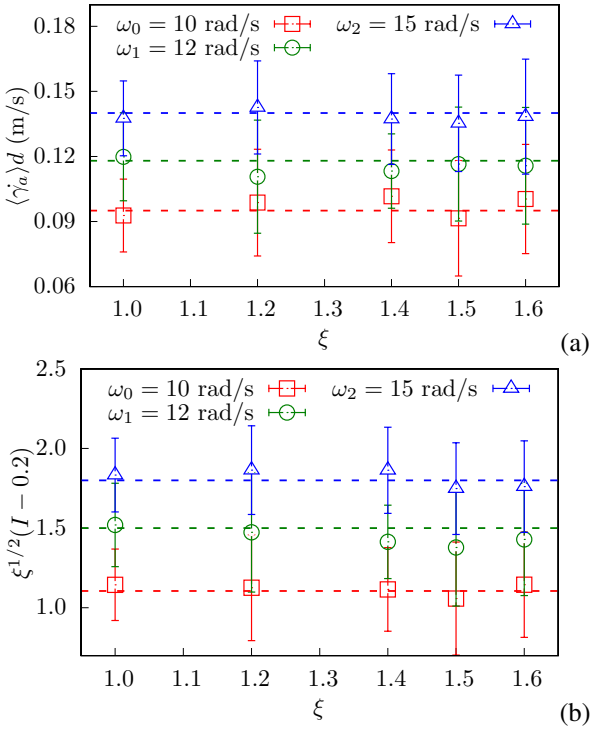

Figure 17: The evolution of relative velocity $\langle\dot{\gamma}_a\rangle d$ and inertial number I inside active layer as a function of coarsening factor ξ. Error bars represent standard deviation.

agreement with the scaling law of Eq. (7). The proposed scaling law also implies that changing particle size can lead to a change of flow regime. Hence, the range of values of parameters for which the system is in the cascading regime varies with particle size. This issue and particle size dependence of thickness ratio h_a/h_b and slope ratio θ_{max}/θ_m can be mitigated by applying a scale factor $\xi^{1/2}$ to rotation speed ω which leads to the multiplication of shear rates by a factor $\xi^{1/2}$, making them independent of coarsening factor. This solution can be applied to the simulations of industrial-scale drums with a reduced number of coarser grains for the sake of computational efficiency.

It is also worth noting that the assumption of the invariance of velocity field may seem to contradict the evolution of flow geometry as observed in Fig. 4. Indeed, the particle velocities can not be strictly compared between the two configurations. The issue is that the surface shape is a free parameter in drum flow. We showed that the relative velocity v_r near drum wall and the total kinetic energy are indeed invariants of particle coarsening (see Fig. 16). This suggest that we may adopt this weaker form of invariance when the geometrical configuration varies with particle coarsening. In other words, the particle coarsening analysis can be applied to the mean flow variables rather than full field variables.

6. Conclusions

In this paper, we used particle dynamics simulations to analyze granular flows composed of octahedral particles in 3D rotating drums for a range of control parameters for which the flow remains in the cascading regime, characterized by dense flows of particles with a curved free surface. A major effect of angular particle shape is the absence of particle slippage at the drum wall, which is commonly observed in drum flows of spherical particles. For this reason, the steady state is characterized by a full balance between flow rates in the passive upward flow and active downward flow layers independently of the values of system parameters such as drum size and rotation speed.

A detailed parametric study was carried out by varying independently drum diameter D, particle diameter d, rotation speed ω, and filling degree J. We showed that the free surface curvature, inertial active flow thickness, and shear velocity are unique linear functions of a scaling parameter $\Gamma = \mathrm{Fr}^{1/2}(D/d)^{1/2}J^{1/4}$, which combines the Froude number $\mathrm{Fr}=D\omega^2/2g$, size ratio D/d, and filling degree J. We argued that this scaling is fully consistent with a particle-coarsening analysis in which the flow scale variables are assumed to be constant and independent of particle size d. We also briefly compared our data with those obtained for flows of spherical particles in a drum.

Further work is necessary to extend the proposed scaling to other particle shapes and to perform a full comparison with drum flows of spherical particles. We are also interested in the effect of both friction coefficient between particles and particle shape angularity on the scaling and crossover from rolling to cascading and from cascading to cataracting regimes. Another important direction of research concerns the effects of size polydispersity and particle breakage on the scaling behavior. While we expect that the general scaling proposed in this paper will not be affected, the numerical parameters involved in

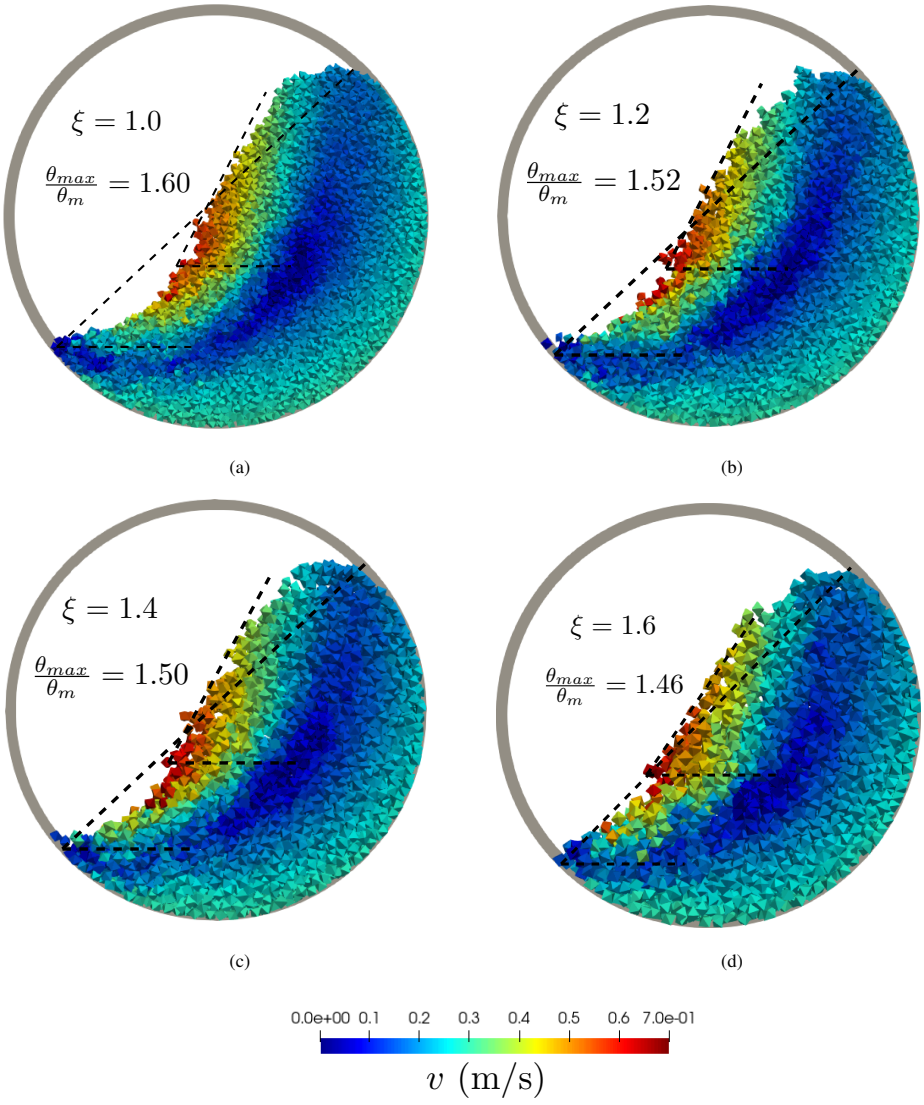

Figure 18: Snapshot of particles and their velocities in rotating drum for different particle coarsening factors ξ for constant filling degree $J = 0.4$, drum diameter $D = 40$ mm, and rotation speed $\omega = 15$ rad/s. Color bar indicates particle velocities. The values of slope ratios are averages in steady flow.

the expressions of flow variables as a function of the scaling parameter may well depend on size polydispersity or evolve with particle breakage. Actually, this scaling provides also a general framework for quantifying such effects.

Last but not least, the findings discussed in this paper suggest new experiments. The flow variables such as slope ratio and thickness ratio are easy to measure using particle tracking. The simple relations between these variables suggested by our simulations, such as the relations (8) and (10), can therefore be checked by experiments using model particles of octahedral shape. By performing experiments with different particle sizes, it is also possible to investigate the effect of particle size through the scaling parameter Γ for different flow variables. For example, relation (8) predicts that the surface curvature increases with increasing ratio D/d. Experiments can be used to validate this trend and to determine whether it holds for large values of D/d and evaluate its limits. We believe that the scaling proposed in this paper holds also for other particle shapes such as elongated particles. However, due to the effect of particle shape on the angle of repose, the numerical values of parameters involved in the relations derived in this paper may change with particle shape. The effect of particle shape can be investigated in parallel by both simulations and experiments. We currently develop new experiments in the geometry of rotating drum with the goal of performing a detailed comparison between experiments and the findings of this paper. The uncertainties associated with possible code-level errors or numerical model parameters can also be evaluated within this project.

Acknowledgments

We warmly thank Luisa Orozco for providing the data of spherical particles. The authors acknowledge financial support by SIFCO project (CEA), EDF, and ORANO.

References

[1] L. Orozco, J.-Y. Delenne, P. Sornay, F. Radjai, Rheology and scaling behavior of cascading granular flows in rotating drums, Journal of Rheology 64 (2020) 915–931.

[2] I. Govender, Granular flows in rotating drums: A rheological perspective, Minerals Engineering 92 (2016) 168–175.
URL https://www.sciencedirect.com/science/article/pii/S0892687516300474

[3] Y. Ding, J. P. K. Seville, R. Forster, D. Parker, Solids motion in rolling mode rotating drums operated at low to medium rotational speeds, Chemical Engineering Science 56 (2001) 1769–1780.

[4] A. Aissa, C. Duchesne, D. Rodrigue, Transverse mixing of polymer powders in a rotary cylinder part i: Active layer characterization, Powder Technology 219 (2012) 193–201.

[5] J. Mellmann, The transverse motion of solids in rotating cylinders–forms of motion and transition behavior, Powder Technology 118 (3) (2001) 251–270.
URL https://www.sciencedirect.com/science/article/pii/S0032591000004022

[6] E. Alizadeh, F. Bertrand, J. Chaouki, Characterization of mixing and size segregation in a rotating drum by a particle tracking method, AIChE Journal 59 (Jun. 2013).

[7] N. Govender, A dem study on the thermal conduction of granular material in a rotating drum using polyhedral particles on gpus, Chemical Engineering Science 252 (2022) 117491.
URL https://www.sciencedirect.com/science/article/pii/S0009250922000756

[8] R. Y. Yang, A. B. Yu, L. McElroy, J. Bao, Numerical simulation of particle dynamics in different flow regimes in a rotating drum, Powder Technology 188 (2) (2008) 170–177.
URL https://www.sciencedirect.com/science/article/pii/S0032591008002167

[9] A. V. Orpe, D. V. Khakhar, Scaling relations for granular flow in quasi-two-dimensional rotating cylinders, Phys. Rev. E 64 (3) (2001) 031302.
URL https://link.aps.org/doi/10.1103/PhysRevE.64.031302

[10] G. Félix, V. Falk, U. D'Ortona, Granular flows in a rotating drum: the scaling law between velocity and thickness of the flow, The European Physical Journal E 22 (1) (2007) 25–31.
URL https://doi.org/10.1140/epje/e2007-00002-5

[11] F. Pignatel, C. Asselin, L. Krieger, I. C. Christov, J. M. Ottino, R. M. Lueptow, Parameters and scalings for dry and immersed granular flowing layers in rotating tumblers, Phys. Rev. E 86 (1) (2012) 011304.
URL https://link.aps.org/doi/10.1103/PhysRevE.86.011304

[12] I. Govender, M. C. Richter, A. N. Mainza, D. N. De Klerk, A positron emission particle tracking investigation of the scaling law governing free surface flows in tumbling mills, AIChE J. 63 (3) (2017) 903–913.
URL https://doi.org/10.1002/aic.15453

[13] N. Taberlet, P. Richard, E. John Hinch, S shape of a granular pile in a rotating drum, Phys. Rev. E 73 (5) (2006) 050301.
URL https://link.aps.org/doi/10.1103/PhysRevE.73.050301

[14] A. Jarray, V. Magnanimo, S. Luding, Wet granular flow control through liquid induced cohesion, Continuous Manufacturing/Processing 341 (2019) 126–139.
URL https://www.sciencedirect.com/science/article/pii/S0032591018301669

[15] P. W. Cleary, G. Metcalfe, K. Liffman, How well do discrete element granular flow models capture the essentials of mixing processes?, Applied Mathematical Modelling 22 (12) (1998) 995–1008.
URL https://www.sciencedirect.com/science/article/pii/S0307904X9810032X

[16] P. W. Cleary, Dem simulation of industrial particle flows: case studies of dragline excavators, mixing in tumblers and centrifugal mills, Powder Technology 109 (1) (2000) 83–104.
URL https://www.sciencedirect.com/science/article/pii/S0032591099002296

[17] P. W. Cleary, The effect of particle shape on simple shear flows, WCPT5 179 (3) (2008) 144–163.
URL https://www.sciencedirect.com/science/article/pii/S0032591007003038

[18] G. Lu, J. R. Third, C. R. Müller, Discrete element models for non-spherical particle systems: From theoretical developments to applications, Chemical Engineering Science 127 (2015) 425–465.
URL https://www.sciencedirect.com/science/article/pii/S0009250914007040

[19] N. Govender, D. N. Wilke, C.-Y. Wu, R. Rajamani, J. Khinast, B. J. Glasser, Large-scale gpu based dem modeling of mixing using irregularly shaped particles, Advanced Powder Technology 29 (10) (2018) 2476–2490.
URL https://www.sciencedirect.com/science/article/pii/S0921883118303054

[20] H. Ma, Y. Zhao, Modelling of the flow of ellipsoidal particles in a horizontal rotating drum based on dem simulation, Chemical Engineering Science 172 (2017) 636–651.
URL https://www.sciencedirect.com/science/article/pii/S0009250917304645

[21] S. Y. He, J. Q. Gan, D. Pinson, Z. Y. Zhou, Particle shape-induced radial segregation of binary mixtures in a rotating drum, Continuous Manufacturing/Processing 341 (2019) 157–166.
URL https://www.sciencedirect.com/science/article/pii/S0032591018304431

[22] S. Y. He, J. Q. Gan, D. Pinson, A. B. Yu, Z. Y. Zhou, Particle shape-induced axial segregation of binary mixtures of spheres and ellipsoids in a rotating drum, Chemical Engineering Science 235 (2021) 116491.
URL https://www.sciencedirect.com/science/article/pii/S0009250921000567

[23] Y. Mori, M. Sakai, Advanced dem simulation on powder mixing for ellipsoidal particles in an industrial mixer, Chemical Engineering Journal 429 (2022) 132415.
URL https://www.sciencedirect.com/science/article/pii/S1385894721039930

[24] O. Dubé, E. Alizadeh, J. Chaouki, F. Bertrand, Dynamics of non-spherical particles in a rotating drum, Chemical Engineering Science 101 (2013) 486–502.
URL https://www.sciencedirect.com/science/article/pii/S0009250913005034

[25] G. G. Pereira, P. W. Cleary, Segregation due to particle shape of a granular mixture in a slowly rotating tumbler, Granular Matter 19 (2) (2017) 23.
URL https://doi.org/10.1007/s10035-017-0708-7

[26] S. Ji, S. Wang, Z. Zhou, Influence of particle shape on mixing rate in rotating drums based on super-quadric dem simulations, Advanced Powder Technology 31 (8) (2020) 3540–3550.
URL https://www.sciencedirect.com/science/article/pii/S0921883120303307

[27] M. H. Abbaspour-Fard, Theoretical validation of a multi-sphere, discrete element model suitable for biomaterials handling simulation, Biosystems Engineering 88 (2) (2004) 153–161.
URL https://www.sciencedirect.com/science/article/pii/S1537511004000492

[28] A. D. Rakotonirina, J.-Y. Delenne, F. Radjai, A. Wachs, Grains3d, a flexible dem approach for particles of arbitrary convex shape–part iii: extension to non-convex particles modelled as glued convex particles, Computational Particle Mechanics 6 (1) (2019) 55–84.
URL https://doi.org/10.1007/s40571-018-0198-3

[29] J. Hlosta, L. Jezerská, J. Rozbroj, D. Žurovec, J. Nečas, J. Zegzulka, Dem investigation of the influence of particulate properties and operating conditions on the mixing process in rotary drums: Part 1–determination of the dem parameters and calibration process (2020).

[30] D. Höhner, S. Wirtz, V. Scherer, A study on the influence of particle shape and shape approximation on particle mechanics in a rotating drum using the discrete element method, Powder Technology 253 (2014) 256–265.
URL https://www.sciencedirect.com/science/article/pii/S0032591013007067

[31] N. Gui, X. Yang, J. Tu, S. Jiang, Z. Zhang, Numerical simulation of tetrahedral particle mixing and motion in rotating drums, Particuology 39 (2018) 1–11.
URL https://www.sciencedirect.com/science/article/pii/S1674200117301773

[32] N. Govender, P. W. Cleary, D. N. Wilke, J. Khinast, The influence of

faceted particle shapes on material dynamics in screw conveying, Chemical Engineering Science 243 (2021) 116654.
URL https://www.sciencedirect.com/science/article/pii/S0009250921002190

[33] N. Govender, R. Kobyłka, J. Khinast, The influence of cohesion on polyhedral shapes during mixing in a drum, Chemical Engineering Science 270 (2023) 118499.
URL https://www.sciencedirect.com/science/article/pii/S0009250923000556

[34] A. López, V. Vivacqua, R. Hammond, M. Ghadiri, Analysis of screw feeding of faceted particles by discrete element method, Powder Technology 367 (2020) 474–486.
URL https://www.sciencedirect.com/science/article/pii/S0032591020302783

[35] V. Richefeu, M. S. El Youssoufi, F. Radjaï, Shear strength properties of wet granular materials, Phys. Rev. E 73 (5) (2006) 051304.
URL https://link.aps.org/doi/10.1103/PhysRevE.73.051304

[36] I. Agnolin, J.-N. Roux, Internal states of model isotropic granular packings. i. assembling process, geometry, and contact networks, Physical Review E 76 (6) (2007) 061302.

[37] E. Azéma, F. Radjai, F. Dubois, Packings of irregular polyhedral particles: Strength, structure, and effects of angularity, Phys. Rev. E 87 (6) (2013) 062203.
URL https://link.aps.org/doi/10.1103/PhysRevE.87.062203

[38] L. Liu, S. Ji, Bond and fracture model in dilated polyhedral dem and its application to simulate breakage of brittle materials, Granular Matter 21 (3) (2019) 41. doi:10.1007/s10035-019-0896-4.
URL https://doi.org/10.1007/s10035-019-0896-4

[39] F. Radjai, V. Richefeu, Contact dynamics as a nonsmooth discrete element method, Mechanics of Materials - MECH MATER 41 (2009) 715–728.

[40] H. J. Herrmann, J.-P. Hovi, S. Luding, Physics of dry granular media, Vol. 350, Springer Science & Business Media, 2013.

[41] N. V. Brilliantov, F. Spahn, J.-M. Hertzsch, T. Pöschel, Model for collisions in granular gases, Phys. Rev. E 53 (5) (1996) 5382–5392.
URL https://link.aps.org/doi/10.1103/PhysRevE.53.5382

[42] M. Y. Louge, Computer simulations of rapid granular flows of spheres interacting with a flat, frictional boundary, Physics of Fluids 6 (7) (1994) 2253–2269.
URL https://doi.org/10.1063/1.868178

[43] H. Tang, R. Song, Y. Dong, X. Song, Measurement of restitution and friction coefficients for granular particles and discrete element simulation for the tests of glass beads (2019).

[44] J. A. I. N. Nitin, R. M. Ottino, J. M. andLueptow, Effect of interstitial fluid on a granular flowing layer, Journal of Fluid Mechanics 508 (2004) 23–44. doi:10.1017/s0022112004008869.
URL https://www.cambridge.org/core/article/effect-of-interstitial-fluid-on-a-granular-flowing-layer/F75AC98B7771CB79883F00E547EB3B0F

[45] H.-T. Chou, C.-F. Lee, Cross-sectional and axial flow characteristics of dry granular material in rotating drums, Granular Matter 11 (1) (2009) 13–32.
URL https://doi.org/10.1007/s10035-008-0118-y

[46] G. Weir, D. Krouse, P. McGavin, The maximum thickness of upper shear layers of granular materials in rotating cylinders, Chemical Engineering Science 60 (7) (2005) 2027–2035.
URL https://www.sciencedirect.com/science/article/pii/S000925090400925X

[47] D. S. Nasato, C. Goniva, S. Pirker, C. Kloss, Coarse graining for large-scale dem simulations of particle flow - an investigation on contact and cohesion models, New Paradigm of Particle Science and Technology Proceedings of The 7th World Congress on Particle Technology 102 (2015) 1484–1490.
URL https://www.sciencedirect.com/science/article/pii/S187770581500301X

[48] M. Sakai, S. Koshizuka, Large-scale discrete element modeling in pneumatic conveying, Chemical Engineering Science 64 (3) (2009) 533–539.
URL https://www.sciencedirect.com/science/article/pii/S0009250908005228

[49] R. Cai, Y. Zhao, An experimentally validated coarse-grain dem study of monodisperse granular mixing, Powder Technology 361 (2020) 99–111.
URL https://www.sciencedirect.com/science/article/pii/S0032591019308575

[50] Y. Dufresne, M. Boulet, S. Moreau, Energy dissipation and onset of instabilities in coarse-grained discrete element method on homogeneous cooling systems, Physics of Fluids 34 (3) (2022) 033306.
URL https://doi.org/10.1063/5.0083873